## **Solid-State Nuclear Magnetic Resonance Studies of Nanoparticles**

Leah B. Casabianca

Department of Chemistry, Clemson University, Clemson, SC, USA

e-mail: <u>lcasabi@clemson.edu</u>

#### Abstract

In this trends article, we review seminal and recent studies using static and magic-angle spinning solid-state NMR to study the structure of nanoparticles and ligands attached to nanoparticles. Solid-state NMR techniques including one-dimensional multinuclear NMR, cross-polarization, techniques for measuring dipolar coupling and internuclear distances, and multidimensional NMR have provided insight into the core-shell structure of nanoparticles as well as the structure of ligands on the nanoparticle surface. Hyperpolarization techniques, in particular solid-state dynamic nuclear polarization (DNP), have enabled detailed studies of nanoparticle core-shell structure and surface chemistry, by allowing unprecedented levels of sensitivity to be achieved. The high signal-to-noise afforded by DNP has allowed homonuclear and heteronuclear correlation experiments involving nuclei with low natural abundance to be performed in reasonable experimental times, which previously would not have been possible. The use of DNP to study nanoparticles and their applications will be a fruitful area of study in the coming years as well.

#### 1. Introduction

Nanoparticles, defined as particles with dimensions between 1 and 100 nm, are an interesting class of materials having properties intermediate between the molecular and bulk scales. In particular, nanoparticles have a significant fraction of their atoms at the surface. The ease of functionalization of materials such as gold nanoparticles, and the highly reactive surfaces, make nanoparticles ideal heterogeneous catalysts. The possibility of defects at the surface increases the number of possible catalyst sites available on nanoparticles. In biomedicine, nanoparticles have a size that allows them to interact with cells and cross the blood-brain barrier. Thus they have been proposed for use as drug-delivery vehicles, as imaging contrast agents, and as in vivo sensors.

Due to their large size, nanoparticles are not usually amenable to study by solution-state NMR, since their slow molecular tumbling leads to short nuclear  $T_2$  relaxation times and broad lines. Ligands that are strongly bound to the nanoparticle surface will also be invisible in solution-state NMR, unless the ligands have some flexibility that affords additional motion. Thus, most of the characterization of nanomaterials and bound ligands has been done by solid-state NMR. Nanoparticle samples are often also porous, amorphous, contain surface defects, and may have a polydispersity of particle sizes in a given sample. Solid-state NMR is especially helpful in the characterization of nanoparticles in this regard, since it is one of the few techniques capable of providing information on non-crystalline solid materials. The importance and timeliness of atomic-level structural characterization of nanoparticles is highlighted in several recent reviews on solid-state NMR studies of nanoparticles.<sup>8-10</sup>

This review will present seminal papers and recent developments in the field of nanoparticle characterization by solid-state NMR. Solid-state NMR has been used to study the core-shell structure of nanoparticles composed of a variety of inorganic and carbon-based materials. It has also been used extensively to study the structure and dynamics of ligands or catalytic substrates on the surface of nanoparticles. The large surface area of nanoparticles is often enough to overcome the sensitivity limitation of NMR; however, the use of hyperpolarization techniques has

driven the field forward by allowing characterization of small amounts of sample with unprecedented sensitivity. The ability to perform two-dimensional homonuclear and heteronuclear correlation experiments involving traditionally unreceptive nuclei has shed new light on the structure of nanoparticles.

This review is organized as follows: the next section will present studies using primarily one-dimensional multinuclear NMR, which can provide a wealth of information from chemical shifts, linewidths, and peak intensities. Section 3 focuses on solid-state NMR techniques for measuring dipolar coupling and internuclear distances, which have been used to deduce the location of dopants or intercalants into nanoparticles, to study the core-shell structure of nanoparticles, and to determine the structure and packing density of ligands on nanoparticle surfaces. Two-dimensional NMR techniques have also been extensively used to study ligand structure, and are covered in section 4. Section 5 presents "other" traditional NMR techniques that have been used to study nanoparticles, including high resolution magic angle spinning (HR-MAS) and very fast magic angle spinning techniques. Section 6 covers the study of nanomaterials by DNP-enhanced solid-state NMR. Last, section 7 provides a summary and outline of future directions in the field.

#### 2. Multinuclear One-Dimensional NMR

One-dimensional solid-state NMR spectra can provide a wealth of information. Chemical shifts depend on particle size and coordination environment, and can be predicted with computational (including density functional theory, or DFT) methods. Knight shifts become important in metallic nanoparticles. Many nanoparticle samples contain several NMR-active nuclei in the same material (111/113Cd, 31P, 77Se, 17O, etc), so one dimensional static or magic angle spinning (MAS) spectra alone can be used to gain a substantial understanding of nanoparticle structure.

In a beautiful work, Wang et al.<sup>11</sup> used <sup>17</sup>O NMR to study the surface and defect sites of ceria nanoparticles. DFT chemical shift calculations predict distinct <sup>17</sup>O chemical shifts for oxygen on the surface and subsurface layers, which can be observed in experimental spectra of <sup>17</sup>O-labeled ceria nanoparticles annealed at various temperatures. Similar work was done for ceria nanocubes, which expose polar (100) facets.<sup>12</sup> A comparison of calculated and experimental <sup>17</sup>O chemical shifts indicate a significant presence of CeO<sub>4</sub>-terminated surface reconstructions. Quantitative <sup>1</sup>H solid-state NMR was used to quantify the amount of terminal and bridging OH groups on the surface of ceria nanoparticles enriched with <sup>17</sup>O<sub>2</sub> or H<sub>2</sub><sup>17</sup>O. Similar methods were also used to characterize ZrO<sub>2</sub> nanocrystals.<sup>13</sup> These studies demonstrate the incredible sensitivity of <sup>17</sup>O chemical shifts to the local environment, and demonstrate the use of solid-state <sup>17</sup>O NMR as a more general method to study surfaces and defects.

Becerra et al.<sup>14</sup> used <sup>31</sup>P solid-state NMR to determine that trioctylphosphine oxide (TOPO) and trioctylphosphine selenide (TOPSe) form a close-packed structure on the surface of CdSe nanocrystallites, with all Cd sites coordinated. The inhomogeneous linewidth of the <sup>31</sup>P spectra of the capping ligands upon coordination to CdSe nanoparticles indicates that the capping ligands experience a variety of chemical environments on the nanoparticle, leading to a distribution of chemical shifts. Tomaselli et al.<sup>15</sup> observed a downfield chemical shift of the <sup>31</sup>P resonance of TOPO ligands capping InP quantum dots with increasing size of the quantum dot. This shift was attributed to increasing downfield contribution from the paramagnetic shielding as more low-lying excited states are present in larger particles.

Solid-state <sup>13</sup>C NMR has been used to show that nanodiamonds have a core-shell structure, with a crystalline diamond core and paramagnetic defects arranged in a layer 0.4-1 nm from the surface. <sup>16</sup> Although an aromatic shell around nanodiamonds has been proposed in the literature, <sup>17</sup> the amount aromatic carbon in pristine, purified detonation nanodiamond has been

shown to be less than 2% of all carbon.<sup>18</sup> The Panich group has used solid-state NMR, focusing on relaxation and spin diffusion, combined with electron paramagnetic resonance (EPR), to characterize detonation nanodiamonds. This work has been summarized in recent reviews.<sup>19,20</sup>

Ladizhansky and Vega<sup>21</sup> used <sup>113</sup>Cd solid-state NMR to study the location of Co<sup>2+</sup> ions doped into CdS nanoparticles. The spectra of different size nanoparticles indicate a structural transition from zinc blende to wurtzite when the nanoparticle diameter exceeds about 8 nm. Based on the integrated intensities of the different <sup>113</sup>Cd sites upon doping with Co<sup>2+</sup> ions, it was determined that the paramagnetic dopants are homogeneously dispersed within the nanoparticle both in the zinc blende and wurtzite structures.

Faulkner et al.<sup>22</sup> used <sup>1</sup>H and <sup>29</sup>Si MAS NMR, combined with quantum mechanical chemical shift calculations, to characterize nano-silicon. These 40-nm nanoparticles are comprised of a crystalline silicon core and a surface rich in Si-H groups and containing silanols as well. The core and shell are connected by Si-O-Si and Si-Si bonds. Solid-state <sup>13</sup>C NMR spectra of labeled and unlabeled alkylthiol groups on gold nanoparticles indicated that the C<sub>1</sub> and C<sub>2</sub> peaks are heterogeneously broadened, representing a variety of chemical environments present for carbons near the gold surface.<sup>23,24</sup> Similar broadening of the C<sub>1</sub> and C<sub>2</sub> resonances was also observed in solution-state NMR of alkanethiol ligands on nanoparticles.<sup>25</sup>

Ladizhansky, Hodes, and Vega presented several seminal studies on the surface of CdS nanoparticles. The  $^{113}$ Cd solid-state NMR spectrum of CdS nanoparticles consists of a sharp resonance attributed to the core Cd atoms and a broad band corresponding to surface Cd sites. This broad band spans a chemical shift region incorporating cadmium bound to sulfur and oxygen, and is consistent with a range of chemical environments for the surface Cd groups (some are expected to be oxidized and some bound to S-O). The broad peak due to surface cadmium atoms also has a shorter  $T_1$  relaxation time than the peak corresponding to the core cadmium sites, as expected due to kinetics and dipolar interactions with protons in the surface cadmium sites.  $^{26}$ 

The <sup>1</sup>H solid-state NMR spectrum of CdS nanoparticles that were precipitated from solution<sup>27</sup> consists of peaks at 4.2 and 6.1 ppm, corresponding to bound water molecules associated with a sulfur site and a cadmium site, respectively. An additional peak at 1.9 ppm is attributed to hydroxyl protons. Sideband analysis and two-dimensional exchange spectroscopy indicate that different molecules in each site exchange rapidly and experience molecular reorientation, whereas exchange between molecules among the different sites occurs on a timescale longer than 50 ms. Based on these results, the authors conclude that the most likely scenario for the structure of water bound to the CdS nanoparticle surface is that of water adsorbed in isolated islands of Cd-bound and S-bound water.

Solid-state NMR studies have provided important insight into nanoparticle catalysts. Peng et al.<sup>28</sup> cleverly used changes in <sup>31</sup>P chemical shift of a reporter molecule, trimethylphosphine, to examine the surface of different facets of ZnO nanocrystals with different morphologies (nanoplates, nanorods, and nanopowders). With the help of DFT calculations, different <sup>31</sup>P chemical shifts were assigned to trimethylphosphine adsorbed to different surface structures on different facets of the ZnO surface, and integration of the different <sup>31</sup>P NMR peaks indicates the proportion of each facet that is exposed in each of the different morphologies. By comparing the different amounts of OH versus vacancy sites for the different morphologies with the catalytic activity of the respective morphologies, they found that OH sites may be more important to catalytic activity than oxygen vacancies. This work has implications for the use of metal oxide nanoparticles in personal care products, such as sun creams, since the nanoparticles have a high concentration of surface OH sites, which can easily photocatalyze the formation of radicals.

Rothermel et al.<sup>29</sup> used <sup>13</sup>C and <sup>31</sup>P MAS NMR to show that the 1,4-Bis(diphenylphosphino) butane capping agent remains on the surface of metal nanoparticles, even after several cycles of catalyzing the deuteration reaction of aliphatic substrates with addition of D<sub>2</sub> gas.

Guo et al.<sup>30</sup> used a combination of solid-state NMR and Fourier transform infrared spectroscopy to show that fumed silica nanoparticles catalyze the reaction of alanine to the cyclic alanine anhydride with a catalytic yield approaching 100%. By contrast, the same reaction catalyzed by colloidal silica nanoparticles has a yield closer to 50%. These results are interesting to the study of prebiotic chemistry as the condensation of alanine to alanine anhydride represents formation of a peptide bond, and the catalysis of this reaction by a mineral (silica) could explain how the first peptide bonds formed.

Chemical shift anisotropy (CSA) is an important parameter in solid-state NMR. The presence of chemical shift anisotropy indicates departure from cubic symmetry in the chemical environment of the nucleus. This has been shown in <sup>113</sup>Cd and <sup>77</sup>Se spectra of CdSe nanoparticles. <sup>31</sup> The CSA also reports on the size of metal oxide nanoparticles. As the nanoparticles become smaller, the NMR linewidth is expected to increase, and the CSA is expected to become more asymmetric. <sup>32,33</sup>

Cross-polarization (CP) from nuclei that are known to be located exclusively on the nanoparticle surface can be used to selectively observe NMR spectra of nuclei in close proximity to the nanoparticle surface. For example, Figure 1 shows how CP from <sup>1</sup>H nuclei located at the surface of silicon nanoparticles can be used to deduce the core-shell structure of these nanoparticles.<sup>34</sup> As the CP mixing time increases, the <sup>29</sup>Si NMR spectrum begins to show narrow features, which are attributed to quasi-ordered silicon sites in the subsurface, superimposed on the broad resonance that is attributed to the disordered surface. By contrast, the direct-polarization <sup>29</sup>Si NMR spectrum is dominated by the narrow resonance that is attributed to Si in a well-ordered environment in the nanoparticle core.

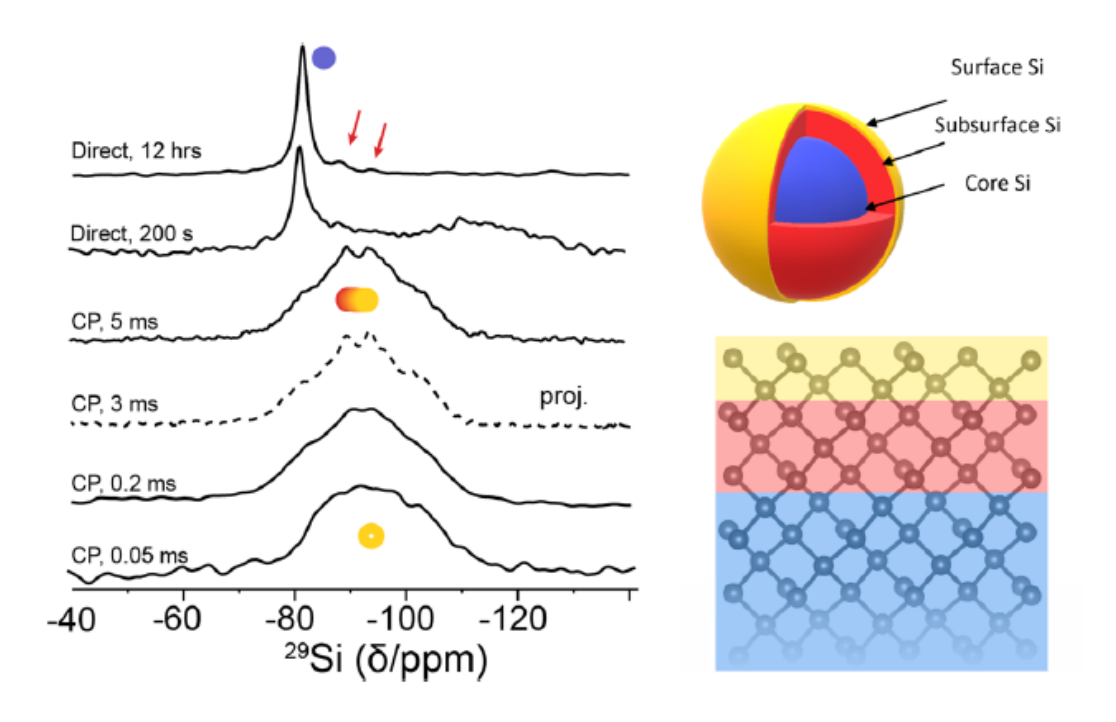


*Figure 1.* Use of cross-polarization to differentiate surface and subsurface Si sites from core Si sites in 64-nm silicon nanoparticles. Reprinted with permission from Thiessen, A. N.; Ha, M.; Hooper, R. W.; Yu, H.; Oliynyk, A. O.; Veinot, J. G. C.; Michaelis, V. K. Silicon Nanoparticles: Are They Crystalline from the Core to the Surface?, *Chem. Mater.* **2019**, *31*, 678-688. Copyright 2019 American Chemical Society.

Cross-polarization magic angle spinning (CP-MAS) has similarly been used to selectively observe the <sup>31</sup>P NMR spectra of phosphorus atoms close to the surface of InP quantum dots<sup>35</sup> and TOPO-passivated InP quantum dots<sup>15</sup> Surface-selective techniques have also been highly used in combination with solid-state dynamic nuclear polarization, as will be discussed in section 6.

Lucier et al.<sup>36</sup> used a clever set of static and MAS <sup>19</sup>F-<sup>89</sup>Y CP experiments to enhance the sensitivity and observe <sup>89</sup>Y NMR in yttrium fluoride nanoparticles. Based on integrated intensities as a function of nanoparticle size, the two <sup>89</sup>Y signals can be assigned to core and surface yttrium sites. Additionally, <sup>19</sup>F MAS NMR indicated three distinct <sup>19</sup>F sites, all of which are in chemical environments that are different from that of <sup>19</sup>F in bulk YF<sub>3</sub>.

### 3. Measurement of Internuclear Distances

A major strength of solid-state NMR is that dipolar coupling can be measured through techniques such as rotational echo double resonance (REDOR)<sup>37</sup> and rotational resonance, and these dipolar couplings can be converted to internuclear distances. Distances derived from solid-state NMR measurements are useful not only for deducing core-shell structure of the nanoparticles themselves, but have also been especially useful in deducing the structure of ligands on the nanoparticle surfaces. Distances have been measured between nuclei in ligands and the nanoparticle surface to confirm ligand attachment, and distances between nuclei in different ligands have been used to deduce packing density and structure.

Avadhut et al.<sup>38</sup> used <sup>119</sup>Sn{<sup>1</sup>H} C-REDOR and <sup>19</sup>F{<sup>1</sup>H} C-REDOR experiments to measure <sup>19</sup>F-<sup>119</sup>Sn distances in fluorine-doped SnO<sub>2</sub> nanoparticles. From the observed internuclear distances, combined with <sup>119</sup>Sn{<sup>19</sup>F} CP-MAS NMR, <sup>19</sup>F-<sup>19</sup>F correlation experiments, and quantum chemical calculations, they deduced that fluorine atoms are situated within the nanoparticle core, not localized to the surface. Fluorine atoms occupy an oxygen vacancy, with only one F atom bound to each Sn atom, and fluorine atoms tend to cluster at grain boundaries.

<sup>13</sup>C{<sup>19</sup>F} REDOR has been used<sup>39</sup> to determine the location of cholic acid guest molecules that have been adsorbed into shell cross-linked nanoparticles composed of poly(4-fluorostyrene)-block-poly(acrylic acid) copolymers. These nanoparticles have a core-shell morphology, and the REDOR NMR results indicate that no cholic acid molecules are located in the core, 28% of the cholic acid molecules are located near the core-shell interface, and 72% of the cholic acid molecules are located more than 25Å from the core-shell interface.

Rotational resonance experiments were used to measure internuclear distances between  $^{13}\text{C}$  labeled sites in amyloid-like peptides as they form self-assembled monolayers on the surface of gold nanoparticles.  $^{40}$  The peptide CFGAILSS is based on the FGAIL sequence of human islet polypeptide amylin, and spontaneously forms fibrils with an antiparallel  $\beta$ -sheet structure in solution. Another peptide studied, CALNN, does not spontaneously form fibrils in solution. When CGFAILSS is adsorbed on the surface of gold nanoparticles, the measured  $^{13}\text{C}'$ - $^{13}\text{C}_{\alpha}$  distance of 4.9  $\pm$  0.3 Å indicates that the peptides do not form  $\beta$ -sheets, but instead are oriented in an inregister, parallel arrangement. On the other hand, no intermolecular dipolar coupling was observed between  $^{13}\text{C}'$  and  $^{13}\text{C}_{\alpha}$  for the CALNN peptide forming self-assembled monolayers on the same size gold nanoparticles. The difference in dipolar coupling measured through rotational resonance indicates that the two peptides form structurally-different self-assembled monolayers on the gold surface.

Gutmann et al.<sup>41</sup> used <sup>31</sup>P-<sup>13</sup>C REDOR to investigate the arrangement of phosphine ligands and reporter CO molecules on the surface of phosphine-stabilized Ru nanoparticles. For the well-characterized system, Ru nanoparticles functionalized with 1,3,5-triaza-7-phosphaadamantane, the nearest-neighbor <sup>31</sup>P-<sup>13</sup>C distance was found to be 3.1Å, in good agreement with DFT calculations. For another system, Ru nanoparticles functionalized with triphenylphosphine, side reactions led to a variety of surface functional groups, including PPh<sub>3</sub> and PCy<sub>3</sub> ligands, as evidenced by a dispersity of <sup>31</sup>P-<sup>13</sup>C distances, between 3 and 4Å.

In a beautiful work by Abraham et al.,  $^{42}$  REDOR solid-state NMR was used to examine the binding of cysteine on the surface of gold nanoparticles. The full  $^{13}$ C solid-state NMR spectrum of cysteine interacting with gold nanoparticles consists of a broad resonance that can be deconvoluted into four peaks, corresponding to two different orientations of the  $\beta$  and  $\gamma$  carbons of cysteine. Intensities of peaks in the reduced REDOR spectrum were used to assign these four peaks. Based on the chemical shifts of the assigned peaks, it was concluded that there are two different chemical environments of cysteine interacting with the nanoparticle surface. The first surface layer binds to the gold through the cysteine sulfur, with the carboxylate groups of cysteine extending out from the surface. The second cysteine layer then interacts with the first layer through hydrogen bonds.

Kurihara et al.<sup>43</sup> used a clever combination of <sup>15</sup>N-<sup>113</sup>Cd J-single quantum filtered (J-1QF) experiments, which report on through-bond interactions through J-couplings, and <sup>15</sup>N-<sup>113</sup>Cd REDOR experiments, which report on through-space interactions through dipolar couplings, to examine amine-nanoparticle interactions in cysteine-capped CdSe magic-sized clusters. They found that ~54% of the cysteine amines in solution were located within close spatial proximity to a cadmium atom. Additionally, ~43% of the amines were shown by the J-filtered experiment to have a chemical bond with cadmium, which means that ~11% of the total amines are located

close to the cadmium selenide surface without forming a chemical bond. In later work,<sup>44</sup> they used <sup>1</sup>H, <sup>13</sup>C, and <sup>23</sup>Na solid-state NMR to deduce the structure of cysteine capping: two binding modes are possible – one involving simultaneous sulfur-cadmium and nitrogen-cadmium bonds, and the other involving only sulfur-cadmium bonds.

### 4. Multidimensional NMR

As with all NMR studies, the characterization of nanoparticles by solid-state NMR benefits from the improved resolution and information content of multidimensional NMR experiments. Heteronuclear correlation (HETCOR) experiments are especially useful for examining correlations between nuclei in the nanoparticle and attached ligands. Capping ligands on the nanoparticle surface are useful for controlling growth of nanoparticles during synthesis, stabilizing the nanoparticles in solution, and preventing dissolution or aggregation. Ligands can also affect the resulting structure and optical properties of the nanoparticle.

Berrettini et al.<sup>48</sup> used CP-MAS <sup>113</sup>Cd and <sup>77</sup>Se NMR to examine the structure of 2-nm CdSe nanoparticles that have been capped with hexadecylamine (HDA) ligand. A comparison of direct polarization (spin echo) experiments and CP experiments indicate that cadmium is less sensitive to changes in chemical environment than the selenium nucleus. Five different selenium sites were observed in the CP-MAS spectrum, which were assigned to edge, vertex, two chemically distinct facet sites, and tetrahedrally-coordinated Se sites one layer deep in the nanoparticle. <sup>1</sup>H-<sup>113</sup>Cd and <sup>1</sup>H-<sup>77</sup>Se HETCOR spectra indicate that HDA and thiophenol ligands are both interacting strongly with cadmium atoms in the nanoparticle. Methylene protons in HDA interact strongly with selenium sites, indicating that the ligand adopts a tilted structure, whereas no interactions between thiophenol protons and selenium atoms are observed. This indicates that thiophenol may be binding to the nanoparticles by occupying a selenium vacancy site. Figure 2 illustrates the binding of HAD and thiophenol to the CdSe surface.

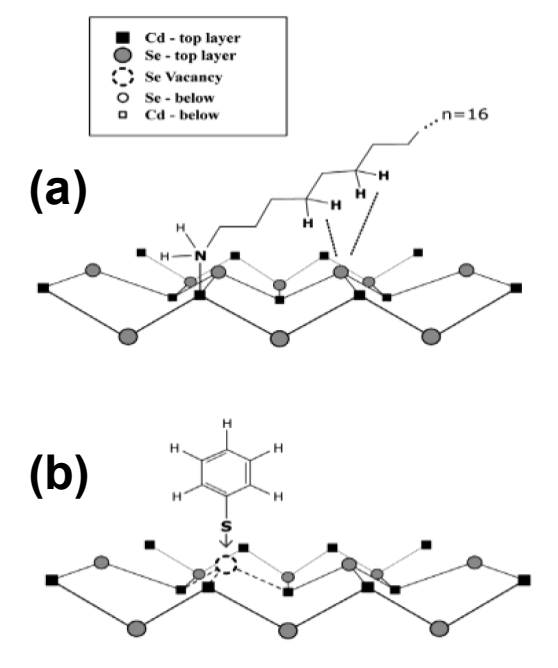
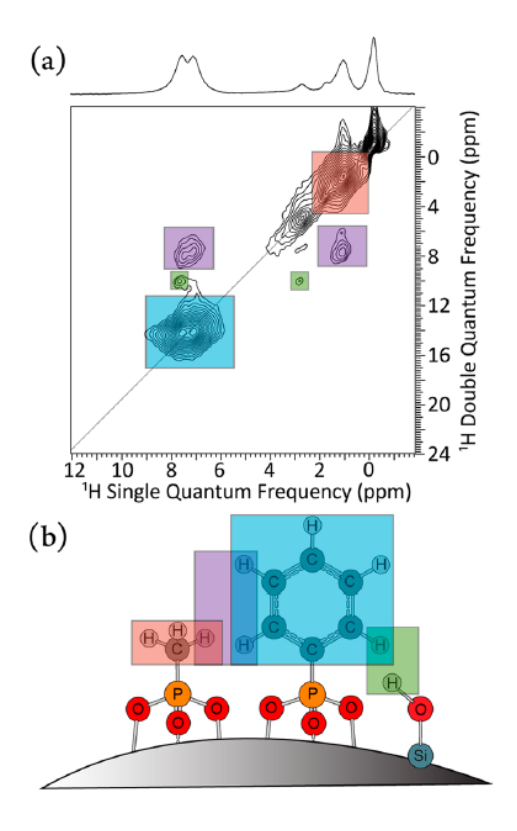


Figure 2. Proposed structures for hexadecylamine and (b) thiophenol interacting with the surface of CdSe nanoparticles. The hexadecylamine adopts a tilted structure, interacting with Se sites, and the thiophenol fills a selenium vacancy site. Reprinted permission from Berrettini, M. G.; Braun, G.: Hu, J. G.: Strouse, G. F. NMR Analysis of Surfaces and Interfaces in 2-nm CdSe, J. Am. Chem. Soc. 2004, 126, 7063-7070. Copyright 2004 American Chemical Society.

Rapp et al.<sup>49</sup> used <sup>13</sup>C–<sup>1</sup>H and <sup>31</sup>P–<sup>1</sup>H indirectly detected heteronuclear correlation (idHETCOR) techniques to confirm that rhodium phosphine ligands had been attached to mesoporous silica

supports. Cano et al.<sup>50</sup> used multidimensional solid-state NMR to characterize the surface sites in iridium catalysts that are selective for the hydrogenation of cinnamalydehyde to the corresponding unsaturated alcohol. <sup>31</sup>P solid-state NMR was used to observe that the secondary phosphine oxide capping ligand on the Ir nanoparticle catalyst can adapt three different binding modes. <sup>13</sup>C solid state NMR was used to explore the free surface sites that are available to coordinate CO, which was used as a probe molecule to examine surface sites of the Ir catalyst nanoparticles. Guo et al. studied the binding of alanine<sup>51</sup> and lysine<sup>52</sup> to the surface of fumed silica nanoparticles using one dimensional solid-state NMR, two-dimensional heteronuclear correlation experiments, and two-dimensional multiple quantum-single quantum spectroscopy experiments.

Multinuclear and multidimensional NMR was used to probe the binding of the ligands methylphosphonic acid (MPA) and phenylphosphonic acid (PPA) on the surface of fumed silica nanoparticles. In the mixed-ligand samples, an exchange spectroscopy (EXSY) spectrum contains cross-peaks between methyl protons of MPA and phenyl protons of PPA, indicating that these two ligands are spatially close. Similarly, H-H double quantum—single quantum (DQ-SQ) back-to-back (BABA) two-dimensional experiments (Figure 3) indicate that the two ligands are strongly dipolar coupled with a maximum average distance of 4.2 ± 0.2Å. This short distance suggests that the two ligands are randomly mixed when binding to the silica surface. When an equal mixture of MPA and PPA was used to functionalize the nanoparticles, MPA was found to preferentially bind. This is attributed to the lower acidity of MPA compared to PPA, making MPA more stable on the SiO<sub>2</sub> surface. In a similar study of mixed phosphonic acids binding to CdSe and ZnS quantum dots, solid-state TNMR was used to quantify remaining phosphonic acid ligands after washing and concomitant quantification of the displaced ligands using solution-state TNMR.



 $^{1}H-^{1}H$ **Figure** 3. double (a) quantum-single quantum (DQ-SQ) back-to-back (BABA) spectrum of a mixed methylphosphonic acid (MPA) and phenylphosphonic acid (PPA)functionalized sample of fumed silica nanoparticles. (b) Structural model showing interactions between protons of MPA, PPA, and surface silanol groups, with colors corresponding to diagonal and cross peaks in the spectrum in (a). Reprinted with permission from Davidowski, S. K.; Holland. G. P. Solid-State NMR Characterization of Mixed Phosphonic Acid Ligand Binding and Organization on Silica Nanoparticles, Langumir 2016, 32, 3253-3261. Copyright 2016 American Chemical Society.

Many inorganic nanoparticles contain quadrupolar nuclei, and multiple quantum magic angle spinning (MQMAS)<sup>55,56</sup> experiments allow the study of half-integer quadrupolar nuclei by removing line broadening due to anisotropy in second-order quadrupolar effects. For example, Goldbourt et al.<sup>57</sup> used 3QMAS and 5QMAS to investigate aluminum that was grafted into the pores of mesoporous silica MCM-41. Al(O-sec-Bu)<sub>3</sub> was grafted into the wide pores of the starting material, and MQMAS experiments were used to deduce the relative amount of aluminum in tetrahedral and octahedral sites.

Avadhut et al.<sup>58</sup> used <sup>27</sup>Al solid-state NMR, as well as correlation experiments between aluminum and carbon and proton, to examine the chemical environment of <sup>27</sup>Al that has been doped into aluminum doped zinc oxide. MQMAS-NMR was used to show that <sup>27</sup>Al peaks are broadened due to second-order quadrupolar broadening and not a distribution of chemical environments. <sup>27</sup>Al{<sup>1</sup>H}-REDOR and <sup>27</sup>Al{<sup>1</sup>H}-phase-shifted recoupling effects a smooth transfer of order (PRESTO)-III experiments indicate short internuclear distances between <sup>27</sup>Al and <sup>1</sup>H coming from organic capping molecules that are present in the nanoparticle shell, indicating that <sup>27</sup>Al is located in the nanoparticle shell. A comparison of experimental <sup>27</sup>Al NMR and calculated chemical shifts, quadrupolar coupling constants, and quadrupolar anisotropies indicates that <sup>27</sup>Al is incorporated into the nanoparticle core as well. Upon reduction, <sup>27</sup>Al experiences a Knight shift, indicating that the reduced nanoparticles obtain some metallic character. These results are important to the use of aluminum doped zinc oxide as a transparent conducting oxide for optoelectronic applications.

## 5. Other Conventional NMR Techniques

Rees et al.<sup>59</sup> used ultrawideline solid-state NMR techniques to collect the solid-state <sup>195</sup>Pt NMR spectrum of various platinum nanoparticles used as catalysts. Experimental lineshapes could be convoluted and combined with theory to determine the number of Pt atoms in the core and shell of the nanoparticle.

Henoumont et al.<sup>60</sup> propose the use of HR-MAS NMR to study ligand bound to the surface of nanoparticles. Zhou et al.<sup>61</sup> used one- and two-dimensional HR-MAS NMR experiments to study organic ligands attached to the surface of gold nanoparticles through thiol groups. They found that signals from protons closer to the gold surface were broadened more than those from protons farther from the gold surface.

Giuntini et al.<sup>62</sup> showed that at high field and very fast magic angle spinning (60KHz), techniques that are usually reserved for solution-state NMR become practical for characterizing proteins that are conjugated to nanoparticles using solid-state NMR. Using <sup>1</sup>H NOSEY, CP-HSQC, and 3D (H)CANH and (H)CONH experiments, they were able to observe spectral changes of the protein *E. coli* asparaginase II (ANSII) upon conjugating it to gold nanoparticles through a poly(ethylene glycol) tether. Kobayashi et al.<sup>63</sup> used <sup>1</sup>H very fast magic angle spinning solid-state NMR to characterize the surface coverage of aminopropyl groups on mesoporous silica nanoparticles (MSN). Through triple quantum-single quantum correlation spectra, they found that the majority of aminopropyl groups were clustered on the MSN surface, even at very low aminopropyl loadings.

# 6. Dynamic Nuclear Polarization-Enhanced Solid-State NMR

 nanoparticles, especially the study of nanoparticle surfaces and experiments which distinguish between the nanoparticle surface and the bulk. These studies have been vital in determining the core-shell structure of several nanoparticles.

Solid-state DNP improves the signal-to-noise of NMR by transferring the high spin polarization of an unpaired electron to nearby nuclei. Depending on the radical EPR linewidth, the polarization transfer may be through the solid effect, the cross effect, and/or thermal mixing. Nuclei that are close enough to the unpaired electron are polarized directly, but these nuclei are often not observed because their relaxation is too fast. Polarization spreads to the bulk sample through spin diffusion. CP can also be combined with DNP, such that a high-gamma nucleus such as H is polarized directly, and polarization is transferred to low-gamma nuclei such as CP. The DNP enhancement factor (usually defined as the ratio between the NMR signal intensity with microwaves on and the signal intensity with microwaves off) is therefore influenced by a combination of several factors, including polarization transfer efficiency, nuclear and electron relaxation times, and spin diffusion. Sample considerations, such as aggregation of radicals and the glass-forming ability of the solvent, can also affect the resulting DNP enhancement factor, since the best polarization transfer is achieved when radicals are homogeneously dispersed among the nuclei to be polarized.

In 2010, Lesage et al.<sup>75</sup> developed surface enhanced NMR spectroscopy (SENS)-DNP. The key to this technique is the incipient wetness impregnation sample preparation strategy. In incipient wetness impregnation, the radical DNP polarizing agent is dissolved in a solvent, minimal amounts of which are then used to wet an insoluble solid that is the target of the DNP-enhanced NMR studies. Because the radicals remain dissolved in the solvent, only nuclei on the surface of the insoluble solid, in contact with the solvent, are hyperpolarized. The SENS-DNP technique was first demonstrated on mesoporous silica because of its high surface area, but since then the SENS-DNP technique has been used to selectively enhance the surface of a variety of materials.<sup>77</sup>

The surface-selective nature of SENS-DNP has been used to examine the core-shell structure of ligand-capped  $Sn/SnO_x$  nanoparticles<sup>78</sup> and a silica-polymer hybrid nanoparticle system composed of a poly(methyl methacrylate) (PMMA) polymer core, a silica shell formed by the hydrolysis and condensation of tetraethylorthosilicate (TEOS), functionalized with trimethylethoxysilane (TMES).<sup>79</sup> SENS-DNP has also been used to determine the location of the cargo (subcore vs surface) in lipid nanoparticles loaded with RNA.<sup>80</sup>

Pinon et al.<sup>81</sup> used relayed DNP to elucidate the core-shell structure of nanocrystals composed of the active pharmaceutical compound P. Lafon et al.<sup>82</sup> have shown that polarization can be transferred from radicals dissolved in a glassing solvent through pores in mesoporous silica nanoparticles through spin diffusion when indirect DNP (polarizing <sup>1</sup>H nuclei followed by spin diffusion and CP to low-gamma nuclei) is used. MAS NMR, CP MAS NMR, and DNP have been used to study the mechanism of CO oxidation supported Pt catalysts.<sup>83</sup>

Johnson et al.<sup>84</sup> were the first to use DNP to study ligands adsorbed on the surface of noble metal nanoparticles used as heterogeneous catalysts. Using SENS-DNP, they were able to record two-dimensional <sup>13</sup>C-<sup>13</sup>C correlation spectra for methionine adsorbed on the nanoparticle surface, which allowed them to elucidate the initial steps of methionine degradation on these catalysts. This approach could have far-reaching implications in catalysis as it allows the study of the initial degradation process, whereas previous experiments have only been able to probe the poisoned catalyst after reaction.

Piveteau et al.<sup>85</sup> pioneered the method of dispersing colloidal quantum dots in mesoporous silica in order to homogeneously disperse the radical polarizing agents and quantum dots. Using mesoporous silica as a sample matrix prevents aggregation of quantum dots, and results in only

a minimal dilution factor. In fact, when comparing the DNP-enhanced signal of QDs in mesoporous silica with the DNP-enhanced signal of dispersed QDs with radical, the overall enhancement was still a factor of 51, indicating that dispersing the radical and QD more than compensated for the dilution factor. Another interesting aspect of this study was that by sequentially filling the mesoporous silica with quantum dots, evaporating the solvent, and then filling the silica with a radical solution, hydrophobic radical solutions could be used to polarize hydrophilic quantum dots and vice versa.

Hanrahan et al.<sup>86</sup> found that by dispersing nanoparticles in hexagonal boron nitride, rather than mesoporous silica, they could obtain even better DNP enhancements. The boron nitride has more favorable dielectric properties than silica and is free of background signal for most semiconductor nanoparticles. Precipitating the nanoparticles and physically mixing the nanoparticle power with boron nitride before impregnating with radical solution led to a reduction in DNP enhancement, but better overall NMR sensitivity due to being able to get more nanoparticles into the rotor. The improved sensitivity allowed the authors to perform two-dimensional NMR experiments, including <sup>113</sup>Cd-<sup>113</sup>Cd and <sup>13</sup>C-<sup>29</sup>Si correlation experiments, on natural abundance samples in a reasonable experimental time. As an example, a <sup>113</sup>Cd-<sup>113</sup>Cd incredible natural abundance double-quantum transfer experiment (INADEQUATE) spectrum, acquired in only 12 hours, is reproduced in Figure 4. The spectrum shows correlation between Cd atoms in the nanoparticle core and at the nanoparticle surface. The ability to record correlation spectroscopy between nuclei that have very low natural abundance is a major advantage of the increased signal intensity from DNP. For example, DNP-enhanced NMR has been used to observe <sup>29</sup>Si-<sup>29</sup>Si correlations in mesoporous silica nanoparticles.<sup>87</sup>

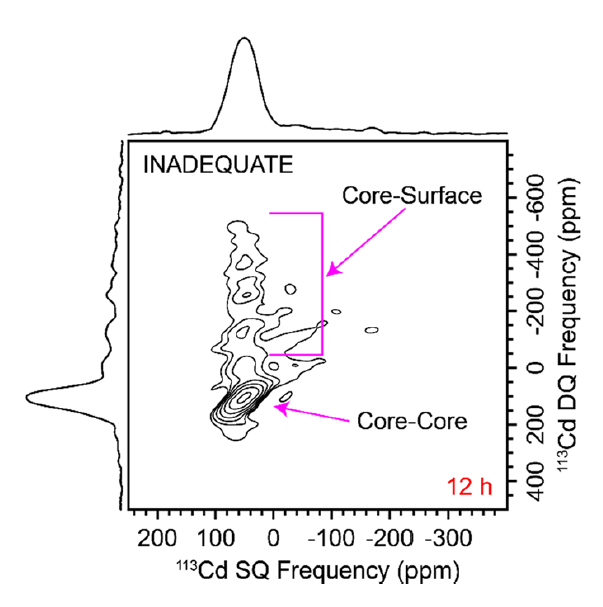


Figure DNP-enhanced <sup>113</sup>Cd-<sup>113</sup>Cd refocused **INADEQUATE-CPMG** 2D correlation spectrum of CdSe quantum dots. The improved sensitivity due to DNP and dispersing nanoparticles in hexagonal boron nitride allowed this spectrum, which shows correlation between core and surface Cd sites, to be collected in 12 hours. Reprinted with permission from Hanrahan, M. P.; Chen, Y.; Blome-Fernández, R.; Stein, J. L.; Pach, G. F.; Adamson, M. A. S.; Neale, N. R.; Cossairt, B. M.; Vela, J.; Rossini, A. J. Structure Probing the Surface Semiconductor Nanoparticles by DNP SENS with Dielectric Support Materials, J. Am. Soc. **2019**, 141, 15532-15546. Copyright 2019 American Chemical Society.

Oxygen is an important atom in biology, materials, and catalysts, yet the extremely low natural abundance of the <sup>17</sup>O nucleus makes oxygen NMR exceedingly challenging. Hope et al. <sup>88</sup> have used DNP-enhanced direct <sup>17</sup>O NMR spectroscopy to study CeO<sub>2</sub> nanoparticles. Oxygen atoms in the first three surface layers can be distinguished on the basis of their <sup>17</sup>O NMR chemical shifts. Within these three layers, the ones closest to the solvent and radicals have the fastest DNP buildup curve, while the oxygen in the core has a significantly slower DNP buildup. The DNP enhancement in the first three surface layers is approximately equal, and the authors attribute this to the more effective DNP polarization transfer concomitant with increased quenching for the surface layers that are closest to the radicals. Indirect DNP, polarizing <sup>1</sup>H nuclei and then

transferring polarization to <sup>17</sup>O using cross-polarization, leads to observation of oxygen in Ce-OH and adsorbed H₂O molecules, but no enhancement of surface or core oxygen.

Previously, <sup>89</sup> we have investigated the effect of size on the DNP polarization efficiency when using the intrinsic paramagnetic defects in diamond as polarizing agents for the <sup>13</sup>C in diamond. We found that we could only obtain significant DNP enhancements for larger (100-nm and larger) diamond particles. For the smaller particles (as small as 5 nm), dangling bonds on the nanoparticle surface led to short electron and nuclear relaxation times. The short electron relaxation time prevented saturation of the electron and the short nuclear relaxation time prevented efficient spin diffusion, both of which are necessary for obtaining high DNP enhancements.

Kwiatkowski et al.<sup>90</sup> found a similar dependence of maximum DNP enhancement on electron and nuclear relaxation times when examining the use of intrinsic defects in silicon nanoparticles to hyperpolarize <sup>29</sup>Si. They found that the ratio of surface defects to surface atoms was a key parameter in achieving the maximum DNP enhancement, and that sample preparation methods, especially ball milling and laser-assisted etching, were promising ways to reliably create nanoparticles with the desired ratio.

On the other hand, when using exogeneous radicals as polarization agents, Akbey et al.<sup>91</sup> found that higher DNP enhancement factors were obtained for smaller silicon nanoparticles. Indirect DNP resulted in higher enhancement factors for the surface silicon sites, while direct CP resulted in higher enhancement factors for the core silicon sites. From the size dependence of the DNP enhancements, the authors were able to estimate the length of a DNP penetration depth of 4.2 nm for indirect DNP and 5.7 nm for direct DNP.

Ha et al.  $^{92}$  compared two DNP methods for hyperpolarizing hydride-terminated silicon nanoparticles: standard indirect DNP, in which the nanoparticles are dispersed in a glassing solvent containing radicals and hydrogen nuclei in the solvent are polarized and polarization is transferred to silicon through CP, and direct DNP of the  $^{29}$ Si nucleus using endogenous radicals (dangling bonds). Endogenous unpaired electrons in the silicon nanoparticles are located mainly in the disordered surface or subsurface layers. The use of endogenous radicals was found to lead to better DNP enhancements, for the primary reason that the exogeneous radicals were destroyed by reaction with the silicon nanoparticle surface within about 30 minutes of sample preparation. On the other hand, using endogenous dangling bonds as DNP polarizing agents, the authors were able to observe  $^{29}$ Si signal from the core, surface, and sub-surface layers. Notably, significant DNP enhancements were found only for the largest nanoparticle (64 nm diameter). In smaller particles (3-21 nm diameters) the majority of  $^{29}$ Si nuclei are too close to dangling bonds on the surface, leading to reduced T1 relaxation times. Short nuclear  $T_1$  relaxion times prevent spin diffusion which is required to obtain DNP enhancement.

Cassidy et al.<sup>93</sup> showed that dangling bonds on the surface of silicon nanoparticles in water can be used as polarizing agents to enhance the signal of both <sup>29</sup>Si in the nanoparticle and <sup>1</sup>H of the water solvent. Two different nuclear spin baths were present – one that consists of nuclei directly polarized by the unpaired electrons, and another that is polarized indirectly through spin diffusion.

Shimon et al.<sup>94</sup> used only the intrinsic dangling bonds located between the silicon and silicon oxide layers of silica nanoparticles to hyperpolarize hydrogen nuclei located near the nanoparticle surface. They found that there are two distinct environments for hydrogen on the nanoparticle surface, both of which lead to NMR linewidths of approximately 5 kHz. The high frequency peak at 10 ppm was attributed to -OH protons, while the low frequency peak was highly shielded, appearing between -19 and -37 ppm with different intensity in different samples. This peak was attributed to a weakly-bound proton species.

Leskes and coworkers<sup>95,96</sup> pioneered a method by which paramagnetic metal ions are doped into inorganic lattices (including lithium ion battery anode materials and phosphor materials) so that these metal ions can act as intrinsic DNP polarization agents. This method may be applicable to nanoparticles in the future.

Presti et al.  $^{97}$  point out that the paramagnetic centers in the dangling bonds on the surface of nanodiamond make the study of nanodiamonds by solid-state NMR similar to the study of any paramagnetic species, with the same inherent opportunities and challenges. The short  $T_1$  relaxation times of nuclei near the surface make CP less efficient, but can contribute to a sensitivity advantage in direct polarization as short relaxation delays can be used to obtain more scans per unit time. The authors found that direct polarization magic angle spinning (DEMAS) was actually more efficient (better sensitivity) than CP-MAS for characterizing organic moieties that are grafted onto the surface of nanodiamonds. The authors also found that conventional DEMAS was preferable to DNP-enhanced DEMAS due to polarization leakage that was driven by the paramagnetic centers on the nanodiamond surface.

### 7. Future Directions

The development and use of DNP for the study of nanoparticles themselves as well as the structure and dynamics of ligands or catalytic substrates adsorbed on the surface of nanoparticles will have far-reaching implications. The increased sensitivity allows the study of low-populated defect sites, surfaces and adsorbed molecules, observation of low-gamma nuclei like <sup>17</sup>O, which comprises metal oxide nanoparticles and is present on the surface of catalysts, and correlation spectra between nuclei that have low natural abundance. As solid-state DNP hardware becomes more commercially available and more groups are able to make use of this technique, nanoparticles with defined surfaces will be able to be prepared, catalytic mechanisms will be deduced, and surface coatings for biocompatible nanoparticles will be optimized. In tandem with advances in DNP methodology and applications, faster MAS and higher magnetic fields will allow solid-state NMR studies of nanoparticles with better resolution.

### **Acknowledgements**

We thank the NSF (CHE-1751529 and CHE-1725919) for partial support of this research. Acknowledgment is made to the Donors of the American Chemical Society Petroleum Research Fund for partial support of this research (58738-DNI6).

### References

- 1. Kobayashi, T.; Perras, F.; Slowing, I. I.; Sadow, A. D.; Pruski, M. Dynamic Nuclear Polarization Solid-State NMR in Heterogeneous Catalysis Research, *ACS Catal.* **2015**, *5*, 7055-7062.
- 2. Lara, S.; Perez-Potti, A.; Herda, L. M.; Adumeau, L.; Dawson, K. A.; Yan, Y. Differential Recognition of Nanoparticle Protein Corona and Modified Low-Density Lipoprotein by Macrophage Receptor with Collagenous Structure, *ACS Nano* **2018**, *12*, 4930-4937.
- 3. Saraiva, C.; Praca, C.; Ferreira, R.; Santos, T.; Ferreira, L.; Bernardino, L. Nanoparticle-mediated brain drug delivery: Overcoming blood-brain barrier to treat neurodegenerative diseases, *J. Control. Rel.* **2016**, *235*, 34-47.

- 4. Hui, Y.; Yi, X.; Hou, F.; Wibowo, D.; Zhang, F.; Zhao, D.; Gao, H.; Zhao, C.-X. Role of Nanoparticle Mechanical Properties in Cancer Drug Delivery, *ACS Nano* **2019**, *13*, 7410-7424.
- 5. Huang, C.-H.; Tsourkas, A. Gd-based macromolecules and nanoparticles as magnetic resonance contrast agents for molecular imaging, *Curr. Top. Med. Chem.* **2013**, *13*, 411-421.
- 6. Bruckman, M. A.; Yu, X.; Steinmetz, N. F. Engineering Gd-loaded nanoparticles to enhance MRI sensitivity via T1 shortening, *Nanotechnol.* **2013**, *24*, 462001.
- 7. Gloag, L.; Mehdipour, M.; Chen, D.; Tilley, R. D.; Gooding, J. J. Advances in the Application of Magnetic Nanoparticles for Sensing, *Adv. Mater.* **2019**, *31*, 1904385.
- 8. Gutmann, T.; Groszewicz, P. B.; Buntkowsky, G. Solid-state NMR of nanocrystals, *Annu. Rep. NMR Spectro.* **2019**, 97, 1-82.
- 9. Marchetti, A.; Chen, J.; Pang, Z.; Li, S.; Ling, D.; Deng, F.; Kong, X. Understanding Surface and Interfacial Chemistry in Functional Nanomaterials via Solid-State NMR, *Adv. Mater.* **2017**, 29, 1605895.
- 10. Epping, J. D.; Chmelka, B. F. Nucleation and growth of zeolites and inorganic mesoporous solids: Molecular insights from magnetic resonance spectroscopy, *Curr. Opin. Colloid In.* **2006**, *11*, 81-117.
- 11. Wang, M.; Wu, X.-P.; Zhang, S.; Zhao, L.; Li, L.; Shen, L.; Gao, Y.; Xue, N.; Guo, X.; Huang, W.; Gan, Z.; Blanc, F.; Yu, Z.; Ke, X.; Ding, W.; Gong, X.-Q.; Grey, C. P.; Peng, L. Identification of different oxygen species in oxide nanostructures with 17O solid-state NMR spectroscopy, *Sci. Adv.* **2015**, *1*, e1400133.
- 12. Chen, J.; Wu, X.-P.; Hope, M. A.; Qian, K.; Halat, D. M.; Liu, T.; Li, Y.; Shen, L.; Ke, X.; Wen, Y.; Du, J.-H.; Magusin, P. C. M. M.; Paul, S.; Ding, W.; Gong, X.-Q.; Grey, C. P.; Peng, L. Polar surface structure of oxide nanocrystals revealed with solid-state NMR spectroscopy, *Nat. Commun.* **2019**, *10*, 5420.
- 13. Shen, L.; Wu, X.-P.; Wang, Y.; Wang, M.; Chen, J.; Li, Y.; Huo, H.; Hou, W.; Ding, W.; Gong, X.-Q.; Peng, L. <sup>17</sup>O Solid-State NMR Studies of ZrO<sub>2</sub> Nanoparticles, *J. Phys. Chem. C* **2019**, *123*, 4158-4167.
- 14. Becerra, L. R.; Murray, C. B.; Griffin, R. G.; Bawendi, M. G. Investigation of the surface morphology of capped CdSe nanocrystallites by <sup>31</sup>P nuclear magnetic resonance, *J. Chem. Phys.* **1994**, *100*, 3297-3300.
- 15. Tomaselli, M.; Yarger, J. L.; Bruchez, M.; Havlin, R. H.; deGraw, D.; Pines, A.; Alivisatos, A. P. NMR study of InP quantum dots: Surface structure and size effects, *J. Chem. Phys.* **1999**, *110*, 8861-8864.
- 16. Fang, X.; Mao, J.; Levin, E. M.; Schmidt-Rohr, K. Nonaromatic Core-Shell Structure of Nanodiamond from Solid-State NMR Spectroscopy, *J. Am. Chem. Soc.* **2009**, *131*, 1426-1435.
- 17. Barnard, A. S.; Sternberg, M. Substitutional Nitrogen in Nanodiamond and Bucky-Diamond Particles, *J. Phys. Chem. B* **2005**, *109*, 17107–17112.
- 18. Cui, J.-F.; Fang, X.-W.; Schmidt-Rohr, K. Quantification of C=C and C=O Surface Carbons in Detonation Nanodiamond by NMR, *J. Phys. Chem. C* **2014**, *118*, 9621-9627.
- 19. Panich, A. M. Nuclear magnetic resonance studies of nanodiamond surface modification, *Diam. Relat. Mater.* **2017**, *79*, 21-31.
- 20. Panich, A. M. Nuclear Magnetic Resonance Studies of Nanodiamonds, *Cr. Rev. Sol. State.* **2012**, *37*, 276-303.

- 21. Ladizhansky, V.; Vega, S. Doping of CdS Nanoparticles by Co<sup>2+</sup> Ions Studied by NMR, *J. Phys. Chem. B* **2000**, *104*, 5237-5241.
- 22. Faulkner, R. A.; DiVerdi, J. A.; Yang, Y.; Kobayashi, T.; Maciel, G. E. The Surface of Nanoparticle Silicon as Studied by Solid-State NMR, *Materials* **2013**, *6*, 18-46.
- 23. Badia, A.; Demers, L.; Dickinson, L.; Morin, F. G.; Lennox, R. B.; Reven, L. Gold-Sulfur Interactions in Alkylthiol Self-Assembled Monolayers Formed on Gold Nanoparticles Studied by Solid-State NMR, *J. Am. Chem. Soc.* **1997**, *119*, 11104-11105.
- 24. Badia, A.; Gao, W.; Singh, S.; Demers, L.; Cuccia, L., Reven, L. Structure and Chain Dynamics of Alkanethiol-Capped Gold Colloids, *Langmuir* **1996**, *12*, 1262-1269.
- 25. Zelakiewicz, B. S.; de Dios, A. C.; Tong, Y. <sup>13</sup>C NMR Spectroscopy of <sup>13</sup>C<sub>1</sub>-Labeled Octanethiol-Protected Au Nanoparticles: Shifts, Relaxations, and Particle-Size Effect, *J. Am. Chem. Soc.* **2003**, *125*, 18-19.
- 26. Ladizhansky, V.; Hodes, G.; Vega, S. Surface Properties of Precipitated CdS Nanoparticles Studied by NMR, *J. Phys. Chem. B* **1998**, *102*, 8505-8509.
- 27. Ladizhansky, V.; Hodes, G.; Vega, S. Solid State NMR Study of Water Binding on the Surface of CdS Nanoparticles. *J. Phys. Chem. B* **2000**, *104*, 1939-1943.
- 28. Peng, Y.-K.; Ye, L.; Qu, J.; Zhang, L.; Fu, Y.; Teixeira, I. F.; McPherson, I. J.; He, H.; Tsang, S. C. E. Trimethylphosphine-Assisted Surface Fingerprinting of Metal Oxide Nanoparticle by 31P Solid-State NMR: A Zinc Oxide Case Study, *J. Am. Chem. Soc.* **2016**, *138*, 2225-2234.
- 29. Rothermel, N.; Röther, T.; Ayvali, T.; Martínez-Prieto, L. M.; Philippot, K.; Limbach, H.-H.; Chaudret, B.; Gutmann, T.; Buntkowsky, G. Reactions of D2 with 1,4-Bis(diphenylphosphino) butane-Stabilized Metal Nanoparticles-A Combined Gas-phase NMR, GC-MS and Solid-state NMR Study, *ChemCatChem* **2019**, *11*, 1465-1471.
- 30. Guo, C.; Jordan, J. S.; Yarger, J. L.; Holland, G. P. Highly Efficient Fumed Silica Nanoparticles for Peptide Bond Formation: Converting Alanine to Alanine Anhydride, *ACS Appl. Mater. Interfaces* **2017**, *9*, 17653-17661.
- 31. Ratcliffe, C. I.; Yu, K.; Ripmeester, J. A.; Zaman, M. B.; Badarau, C.; Singh, S. Solid state NMR studies of photoluminescent cadmium chalcogenide nanoparticles, *Phys. Chem. Chem. Phys.* **2006**, *8*, 3510-3519.
- 32. Aliev, A. E.; Bartók, A. P.; Yates, J. R. Tin chemical shift anisotropy in tin dioxide: On ambiguity of CSA asymmetry derived from MAS spectra, *Solid State Nucl. Mag.* **2018**, *89*, 1-10.
- 33. Tunstall, D. P.; Patou, S.; Liu, R. S.; Kao, Y. H. Size effects in the NMR of SnO<sub>2</sub> powders, *Mater. Res. Bull.* **1999**, *34*, 1513-1520.
- 34. Thiessen, A. N.; Ha, M.; Hooper, R. W.; Yu, H.; Oliynyk, A. O.; Veinot, J. G. C.; Michaelis, V. K. Silicon Nanoparticles: Are They Crystalline from the Core to the Surface?, *Chem. Mater.* **2019**, *31*, 678-688.
- 35. Cros-Gagneux, A.; Delpech, F.; Nayral, C.; Cornejo, A.; Coppel, Y.; Chaudret, B. Surface Chemistry of InP Quantum Dots: A Comprehensive Study, *J. Am. Chem. Soc.* **2010**, *132*, 18147-18157.
- 36. Lucier, B. E. G.; Johnston, K. E.; Arnold, D. C.; Lemyre, J.-L.; Beaupré, A.; Blanchette, M.; Ritcey, A. M.; Schurko, R. W. Comprehensive Solid-State Characterization of Rare Earth Fluoride Nanoparticles, *J. Phys. Chem. C* **2014**, *118*, 1213-1228.

- 37. Gullion, T.; Schaefer, J. Rotational-Echo Double Resonance NMR, *J. Magn. Reson.* **1989**, *81*, 196-200.
- 38. Avadhut, Y. S.; Weber, J.; Hammarberg, E.; Feldman, C.; Schellenberg, I.; Pöttgen, R.; Schmedt af der Günne, J. Study on the Defect Structure of SnO2:F Nanoparticles by High-Resolution Solid-State NMR, *Chem. Mater.* **2011**, *23*, 1526-1538.
- 39. Kao, H.-M.; O'Connor, R. D.; Mehta, A. K.; Huang, H.; Poliks, B.; Wooley, K. L.; Schaefer, J. Location of Cholic Acid Sequestered by Core-Shell Nanoparticles Using REDOR NMR, *Macromolecules* **2001**, *34*, 544-546.
- 40. Shaw, C. P.; Middleton, D. A.; Volk, M.; Lévy, R. Amyloid-Derived Peptide Forms Self-Assembled Monolayers on Gold Nanoparticle with a Curvature- Dependent β-Sheet Structure, *ACS Nano* **2012**, *6*, 1416-1426.
- 41. Gutmann, T.; Bonnefille, E.; Breitzke, H.; Debouttière, P.-J.; Philippot, K.; Ponteau, R.; Buntkowsky, G.; Chaudret, B. Investigation of the surface chemistry of phosphine-stabilized ruthenium nanoparticles an advanced solid-state NMR study, *Phys. Chem. Chem. Phys.* **2013**, *15*, 17383-17394.
- 42. Abraham, A.; Mihaliuk, E.; Kumar, B.; Legleiter, J.; Gullion, T. Solid-State NMR Study of Cysteine on Gold Nanoparticles, *J. Phys. Chem. C* **2010**, *114*, 18109-18114.
- 43. Kurihara, T.; Noda, Y.; Takegoshi, K. Quantitative Solid-State NMR Study on Ligand-Surface Interaction in Cysteine-Capped CdSe Magic-Sized Clusters. *J. Phys. Chem. Lett.* **2017**, *8*, 2555-2559.
- 44. Kurihara, T.; Noda, Y.; Takegoshi, K. Capping Structure of Ligand-Cysteine on CdSe Magic-Sized Clusters, *ACS Omega* **2019**, *4*, 3476-3483.
- 45. Wang, W.; Banerjee, S.; Jia, S.; Steigerwald, M. L.; Herman, I. P. Ligand Control of Growth, Morphology, and Capping Structure of Colloidal CdSe Nanorods, *Chem. Mater.* **2007**, *19*, 2573-2580.
- 46. Huang, J.; Kovalenko, M. V.; Talapin, D. V. Alkyl Chains of Surface Ligands Affect Polytypism of CdSe Nanocrystals and Play an Important Role in the Synthesis of Anisotropic Nanoheterostructures, *J. Am. Chem. Soc.* **2010**, *132*, 15866-15868.
- 47. Frederick, M. T.; Amin, V. A.; Weiss, E. A. Optical Properties of Strongly Coupled Quantum Dot-Ligand Systems, *J. Phys. Chem. Lett.* **2013**, *4*, 634-640.
- 48. Berrettini, M. G.; Braun, G.; Hu, J. G.; Strouse, G. F. NMR Analysis of Surfaces and Interfaces in 2-nm CdSe, *J. Am. Chem. Soc.* **2004**, *126*, 7063-7070.
- 49. Rapp, J. L.; Huang, Y.; Natella, M.; Cai, Y.; Lin, V. S.-Y.; Pruski, M. A solid-state NMR investigation of the structure of mesoporous silica nanoparticle supported rhodium catalysts, *Solid State Nucl. Mag.* **2009**, *35*, 82-86.
- 50. Cano, I.; Martínez-Prieto, L. M.; Fazzini, P. F.; Coppel, Y.; Chaudret, B.; van Leeuwen, P. W. N. M. Characterization of secondary phosphine oxide ligands on the surface of iridium nanoparticles, *Phys. Chem. Chem. Phys.* **2017**, *19*, 21655-21662.
- 51. Guo, C.; Holland, G. P. Alanine Adsorption and Thermal Condensation at the Interface of Fumed Silica Nanoparticles: A Solid-State NMR Investigation, *J. Phys. Chem. C* **2015**, *119*, 25663-25672.
- 52. Guo, C.; Holland, G. P. Investigating Lysine Adsorption on Fumed Silica Nanoparticles, *J. Phys. Chem. C* **2014**, *118*, 25792-25801.

- 53. Davidowski, S. K.; Holland, G. P. Solid-State NMR Characterization of Mixed Phosphonic Acid Ligand Binding and Organization on Silica Nanoparticles, *Langumir* **2016**, *32*, 3253-3261.
- 54. Davidowski, S. K.; Lisowski, C. E.; Yarger, J. L. Characterizing mixed phosphonic acid ligand capping on CdSe/ZnS quantum dots using ligand exchange and NMR spectroscopy, *Magn. Reson. Chem.* **2016**, *54*, 234-238.
- 55. Frydman, L.; Harwood, J. S. Isotropic Spectra of Half-Integer Quadrupolar Spins from Bidimensional Magic-Angle Spinning NMR, *J. Am. Chem. Soc.* **1995**, *117*, 5367-5368.
- 56. Medek, A.; Harwood, J. S.; Frydman, L. Multiple-Quantum Magic-Angle Spinning NMR: A New Method for the Study of Quadrupolar Nuclei in Solids, *J. Am. Chem. Soc.* **1995**, *117*, 12779-12787.
- 57. Goldbourt, A.; Landau, M. V.; Vega, S. Characterization of Aluminum Species in Alumina Multilayer Grafted MCM-41 Using <sup>27</sup>Al FAM(II)-MQMAS NMR, *J. Phys. Chem. B* **2003**, *107*, 724-731.
- 58. Avadhut, Y. S.; Weber, J.; Hammarberg, E.; Feldman, C.; Schmedt auf der Günne, J. Structural investigation of aluminium doped ZnO nanoparticles by solid-state NMR spectroscopy. *Phys. Chem. Chem. Phys.* **2012**. *14*. 11610-11625.
- 59. Rees, G. J.; Orr, S. T.; Barrett, L. O.; Fisher, J. M.; Houghton, J.; Spikes G. H.; Theobald, B. R. C.; Thompsett, D.; Smith, M. E.; Hanna, J. V. Characterisation of platinum-based fuel cell catalyst materials using 195Pt wideline solid state NMR, *Phys. Chem. Chem. Phys.* **2013**, *15*, 17195-17207.
- 60. Henoumont, C.; Laurent, S.; Muller, R. N.; Vaner Elst, L. HR-MAS NMR Spectroscopy: An Innovative Tool for the Characterization of Iron Oxide Nanoparticles Tracers for Molecular Imaging, *Anal. Chem.* **2015**, *87*, 1701-1710.
- 61. Zhou, H.; Du, F.; Li, X.; Zhang, B.; Li, W.; Yan, B. Characterization of Organic Molecules Attached to Gold Nanoparticle Surface Using High Resolution Magic Angle Spinning <sup>1</sup>H NMR, *J. Phys. Chem. C* **2008**, *112*, 19360-19366.
- 62. Giuntini, S.; Cerofolini, L.; Ravera, E.; Fragai, M.; Luchinat, C. Atomic structural details of a protein grafted onto gold nanoparticles, *Sci. Rep.* **2017**, *7*, 17934.
- 63. Kobayashi, T.; Singappuli-Arachchige, D.; Slowing, I. I.; Pruski, M. Spatial distribution of organic functional groups supported on mesoporous silica nanoparticles (2): a study by <sup>1</sup>H triple-quantum fast-MAS solid-state NMR, *Phys. Chem. Chem. Phys.* **2018**, *20*, 22203-22209.
- 64. Rankin, A. G. M.; Trébosc, J.; Pourpoint, F.; Amoureux, J.-P.; Lafon, O. Recent developments in MAS DNP-NMR of materials, *Solid State Nucl. Mag.* **2019**, *101*, 116-143.
- 65. Rossini, A. J. Materials Characterization by Dynamic Nuclear Polarization-Enhanced Solid-State NMR Spectroscopy, *J. Phys. Chem. Lett.* **2018**, *9*, 5150-5159.
- 66. Walker, T. G.; Happer, W. Spin-exchange optical pumping of noble-gas nuclei, *Rev. Mod. Phys.* **1997**, *69*, 629-642.
- 67. Appelt, S.; Baranga, A. B.; Erickson, C. J.; Romalis, M. V.; Young, A. R.; Happer, W. Theory of spin-exchange optical pumping of He-3 and Xe-129, *Phys. Rev. A* **1998**, *58*, 1412-1439.
- 68. Carver, T. R.; Slichter, C. P. Polarization of Nuclear Spins in Metals. *Phys. Rev.* **1953**, 92, 212–213.
- 69. Abragam, A.; Goldman, M. Principles of dynamic nuclear polarisation, *Rep. Prog. Phys.* **1978**, *41*, 395-467.

- 70. Bowers, C. R.; Weitekamp, D. P. Transformation of symmetrization order to nuclear-spin magnetization by chemical-reaction and nuclear-magnetic-resonance *Phys. Rev. Lett.* **1986**, *57*, 2645-2648.
- 71. Bowers, C. R.; Weitekamp, D. P. Para-hydrogen and synthesis allow dramatically enhanced nuclear alignment, *J. Am. Chem. Soc.* **1987**, *109*, 5541-5542.
- 72. Maly, T.; Debelouchina, G. T.; Bajaj, V. S.; Hu, K.-N.; Joo, C.-G.; Mak-Jurkauskas, M. L.; Sirigiri, J. R.; van der Wel, P. C. A.; Herzfeld, J.; Temkin, R. J.; Griffin, R. G. Dynamic nuclear polarization at high magnetic fields, *J. Chem. Phys.* **2008**, *128*, 052211.
- 73. Corzilius, B.; Andreas, L. B.; Smith, A. A.; Ni, Q. Z.; Griffin, R. G. Paramagnet induced signal quenching in MAS–DNP experiments in frozen homogeneous solutions, *J. Magn. Reson.* **2014**, 240, 113-123.
- 74. Hovav, Y.; Feintuch, A.; Vega, S. Dynamic nuclear polarization assisted spin diffusion for the solid effect case, *J. Chem. Phys.* **2011**, *134*, 074509.
- 75. Lesage, A.; Lelli, M.; Gajan, D.; Caporini, M. A.; Vitzthum, V.; Miéville, P.; Alauzun, J.; Roussey, A.; Thieuleux, C.; Medhi, A.; Bodenhausen, G.; Coperet, C.; Emsley, L. Surface Enhanced NMR Spectroscopy by Dynamic Nuclear Polarization, *J. Am. Chem. Soc.* **2010**, *132*, 15459-15461.
- 76. Kobayashi, T.; Lafon, O.; Thankamony, A. S. L.; Slowing, I. I.; Kandel, K.; Carnevale, D.; Vitzthum, V.; Vezin, H.; Amoureux, J.-P.; Bodenhausen, G.; Pruski, M. Analysis of sensitivity enhancement by dynamic nuclear polarization in solid-state NMR: a case study of functionalized mesoporous materials, *Phys. Chem. Chem. Phys.* **2013**, *15*, 5553-5562.
- 77. Rossini, A. J.; Zagdoun, A.; Lelli, M.; Lesage, A.; Copéret, C.; Emsley, L. Dynamic Nuclear Polarization Surface Enhanced NMR Spectroscopy, *Acc. Chem. Res.* **2013**, *46*, 1942-1951.
- 78. Protesescu, L.; Rossini, A. J.; Kriegner, D.; Valla, M.; de Kergommeaux, A.; Walter, M.; Kravchyk, K. V.; Nachtegaal, M.; Stangl, J.; Malaman, B.; Reiss, P.; Lesage, A.; Emsley, L.; Copéret, C.; Kovalenko, M. V. Unraveling the Core-Shell Structure of Ligand-Capped Sn/SnO<sub>x</sub> Nanoparticles by Surface-Enhanced Nuclear Magnetic Resonance, Mössbauer, and X-ray Absorption Spectroscopies, *ACS Nano* **2014**, *8*, 2639-2648.
- 79. Schäfer, T.; Vowinkel, S.; Breitzke, H.; Gallei, M.; Gutmann, T. Selective DNP Signal Amplification To Probe Structures of Core-Shell Polymer Hybrid Nanoparticles, *J. Phys. Chem. C* **2019**, *123*, 644-652.
- 80. Viger-Gravel, J.; Schantz, A.; Pinon, A. C.; Rossini, A. J.; Schantz, S.; Emsley, L. Structure of Lipid Nanoparticles Containing siRNA or mRNA by Dynamic Nuclear Polarization-Enhanced NMR Spectroscopy, *J. Phys. Chem. B* **2018**, *122*, 2073-2081.
- 81. Pinon, A. C.; Skantze, U.; Viger-Gravel, J.; Schantz, S.; Emsley, L. Core-Shell Structure of Organic Crystalline Nanoparticles Determined by Relayed Dynamic Nuclear Polarization NMR, *J. Phys. Chem. A* **2018**, *122*, 8802-8807.
- 82. Lafon, O.; Lilly Thankamony, A. S.; Kobayashi, T.; Carnevale, D.; Vitzthum, V.; Slowing, I. I.; Kandel, K.; Vezin, H.; Amoureux, J.-P.; Bodenhausen, G.; Pruski, M. Mesoporous Silica Nanoparticles Loaded with Surfactant: Low Temperature Magic Angle Spinning 13C and 29Si NMR Enhanced by Dynamic Nuclear Polarization, *J. Phys. Chem. C* **2013**, *117*, 1375-1382.
- 83. Kilmavicius, V.; Neumann, S.; Kunz, S.; Gutmann, T.; Buntkowsky, G. Room temperature CO oxidation catalysed by supported Pt nanoparticles revealed by solid-state NMR and DNP spectroscopy, *Catal. Sci. Technol.* **2019**, *9*, 3743-3752.

- 84. Johnson, R. L.; Perras, F. A.; Kobayashi, T.; Schwartz, T. J.; Dumesic, J. A.; Shanks, B. H.; Pruski, M. Identifying low-coverage surface species on supported noble metal nanoparticle catalysts by DNP-NMR, *Chem. Commun.* **2016**, *52*, 1859-1862.
- 85. Piveteau, L.; Ong, T.-C.; Rossini, A. J.; Emsley, L.; Copéret, C.; Kovalenko, M. V. Structure of Colloidal Quantum Dots from Dynamic Nuclear Polarization Surface Enhanced NMR Spectroscopy, *J. Am. Chem. Soc.* **2015**, *137*, 13964-13971.
- 86. Hanrahan, M. P.; Chen, Y.; Blome-Fernández, R.; Stein, J. L.; Pach, G. F.; Adamson, M. A. S.; Neale, N. R.; Cossairt, B. M.; Vela, J.; Rossini, A. J. Probing the Surface Structure of Semiconductor Nanoparticles by DNP SENS with Dielectric Support Materials, *J. Am. Chem. Soc.* **2019**, *141*, 15532-15546.
- 87. Kobayashi, T.; Singappuli-Arachchige, D.; Wang, Z.; Slowing, I. I.; Pruski, M. Spatial distribution of organic functional groups supported on mesoporous silica nanoparticles: a study by conventional and DNP-enhanced <sup>29</sup>Si solid-state NMR, *Phys. Chem. Chem. Phys.* **2017**, *19*, 1781-1789.
- 88. Hope, M. A.; Halat, D. M.; Magusin, P. C. M. M.; Paul, S.; Peng, L.; Grey, C. P. Surface-selective direct <sup>17</sup>O DNP NMR of CeO<sub>2</sub> nanoparticles, *Chem. Comm.* **2017**, *53*, 2142-2145.
- 89. Casabianca, L. B.; Shames, A. I.; Panich, A. M.; Shenderova, O.; Frydman, L. Factors Affecting DNP NMR in Polycrystalline Diamond Samples, *J. Phys. Chem. C* **2011**, *115*, 19041-19048.
- 90. Kwiatkowski, G.; Polyhach, Y.; Jähnig, F.; Shiroka, T.; Starsich, F. H. L.; Ernst, M.; Kozerke, S. Exploiting Endogenous Surface Defects for Dynamic Nuclear Polarization of Silicon Microand Nanoparticles, *J. Phys. Chem. C* **2018**, *122*, 25668-25680.
- 91. Akbey, Ü.; Altin, B.; Linden, A.; Özçelik, S.; Gradzielski, M.; Oschkinat, H. Dynamic nuclear polarization of spherical nanoparticles, *Phys. Chem. Chem. Phys.* **2013**, *15*, 20706-20716.
- 92. Ha, M.; Thiessen, A. N.; Sergeyev, I. V.; Veinot, J. C. C.; Michaelis, V. K. Endogenous dynamic nuclear polarization NMR of hydride-terminated silicon nanoparticles, *Solid State Nucl. Mag.* **2019**, *100*, 77-84.
- 93. Cassidy, M. C.; Ramanathan, C.; Cory, D. G.; Ager, J. W.; Marcus, C. M. Radical-free dynamic nuclear polarization using electronic defects in silicon, *Phys. Rev. B* **2013**, *87*, 161306.
- 94. Shimon, D.; van Schooten, K. J.; Paul, S.; Peng, Z.; Takahashi, S.; Köckenberger, W.; Ramanathan, C. DNP-NMR of surface hydrogen on silicon microparticles, *Solid State Nucl. Mag.* **2019**, *101*, 68-75.
- 95. Wolf, T.; Kumar, S.; Singh, H.; Chakrabarty, T.; Aussenac, F.; Frenkel, A. I.; Major, D. T.; Leskes, M. Endogenous Dynamic Nuclear Polarization for Natural Abundance 17O and Lithium NMR in the Bulk of Inorganic Solids, *J. Am. Chem. Soc.* **2019**, *141*, 451-462.
- 96. Chakrabarty, T.; Goldin, N.; Feintuch, A.; Houben, L.; Leskes, M. Paramagnetic Metal-Ion Dopants as Polarization Agents for Dynamic Nuclear Polarization NMR Spectroscopy in Inorganic Solids, *ChemPhysChem* **2018**, *19*, 2139-2142.
- 97. Presti, C.; Lilly Thanksamony, A. S.; Alauzun, J. G.; Mutin, P. H.; Carnevale, D.; Lion, C.; Vezin, H.; Laurencin, D.; Lafon, O. NMR and EPR Characterization of Functionalized Nanodiamonds, *J. Phys. Chem. C* **2015**, *119*, 12408-12422.